Emergence of charge order in a staggered loop-current phase of cuprate high-temperature superconductors

W. A. Atkinson[*]

Department of Physics and Astronomy, Trent University, Peterborough, Ontario, Canada K9J7B8

A. P. Kampf[†] and S. Bulut

Theoretical Physics III, Center for Electronic Correlations and Magnetism, Institute of Physics,
University of Augsburg, 86135 Augsburg, Germany

We study the emergence of charge-ordered phases within a π-loop-current (πLC) model for the pseudogap based on a three-band model for underdoped cuprate superconductors. Loop currents and charge ordering are driven by distinct components of the short-range Coulomb interactions: loop currents result from the repulsion between nearest-neighbor copper and oxygen orbitals, while charge order results from repulsion between neighboring oxygen orbitals. We find that the leading πLC phase has an antiferromagnetic pattern similar to previously discovered staggered flux phases, and that it emerges abruptly at hole dopings p below the Van Hove filling. Subsequent charge-ordering tendencies in the πLC phase reveal that diagonal d-charge density waves (dCDWs) are suppressed by the loop currents while axial order competes more weakly. In some cases we find a wide temperature range below the loop-current transition, over which the susceptibility towards an axial dCDW is large. In these cases, short-range axial charge order may be induced by doping-related disorder. A unique feature of the coexisting dCDW and πLC phases is the emergence of an incommensurate modulation of the loop currents. If the dCDW is biaxial (checkerboard) then the resulting incommensurate current pattern breaks all mirror and time-reversal symmetries, thereby allowing for a polar Kerr effect.

I. INTRODUCTION

Charge order is a universal feature of underdoped cuprate high-temperature superconductors. Charge-ordered phases lie in close proximity to antiferromagnetic, spin-glass, and superconducting phases, implying a close competition between the different ordering tendencies. This raises the possibility that some or all of the anomalous properties exhibited by the cuprates are due to multiple competing or coexisting electronic phases.

Originally observed by scanning tunneling spectroscopy in Bi-based cuprates [1–3], charge order was then inferred to exist also in YBa$_2$Cu$_3$O$_{6+x}$, e.g., from magnetotransport [4–6] and magneto-oscillation experiments [7,8], NMR [9,10], and x-ray scattering [11–15]. More recently, charge order has been found in HgBa$_2$CuO$_{4+\delta}$ [16–18] and in the electron-doped compound Nd$_{2-x}$Ce$_x$CuO$_4$ [19].

The charge order has two distinguishing features: it has modulation wave vectors **q** that lie along the crystalline axes (so-called "axial order"), and it has an approximate $d_{x^2-y^2}$ internal structure [2,20–23]. We therefore adopt the notation d-charge density wave (dCDW). In essence, the dCDW can be thought of as a predominant charge transfer between neighboring oxygen p orbitals the amplitude of which is modulated with wave vector **q** [24–27].

This dCDW is distinct from the stripe order found in La-based cuprates. While both are strongest near hole dopings of $p = 0.12$, stripes are characterized by an entanglement of spin and charge degrees of freedom [28] that is absent in the

dCDW phase [29]; additionally, the doping dependence of the density modulations follows an opposite trend in stripe- and charge-ordered materials [29].

Charge order also appears to be distinct from the pseudogap phenomena. Early experiments on YBa$_2$Cu$_3$O$_{6+x}$ [11,12] and Bi$_2$Sr$_{2-x}$La$_x$CuO$_{6+x}$ [30] found that static charge modulations develop at temperatures T_{co} close to the pseudogap onset temperature T^*, and this suggested a cause for the partial destruction of the Fermi surface that characterizes the pseudogap. Furthermore, a recent STM study of Bi$_2$Sr$_2$CaCu$_2$O$_{8+x}$ [31] found a connection between the energy scales of the charge order and the pseudogap. However, systematic studies over a wide doping range in YBa$_2$Cu$_3$O$_{6+x}$ have revealed that the onset of the dCDW at T_{co} varies differently with p than does T^* [14,15]. In addition, the pseudogap was found insensitive to doping with Zn impurities [32–35], while charge order is rapidly quenched [14,36]. Finally, the wave vector associated with the dCDW connects tips of the remnant Fermi arcs in the pseudogap phase; this suggests that charge order is an instability of, rather than the cause of, the Fermi arcs [30]; indeed, theoretical calculations accurately reproduce experimental wave vectors under this assumption [26,37–39].

Most previous theoretical studies of charge order in cuprates are based on one-band spin-fermion models, for which the analog of dCDW order is a bond-order wave [40–44]. These calculations assume that the dominant electron-electron interaction is mediated by a low-energy spin resonance that is peaked at **Q** $= (\pi,\pi)$, and focus on the instabilities generated by this interaction. Several calculations found instabilities towards dCDW states with ordering wave vectors **q** oriented along the Brillouin zone diagonal (so-called "diagonal order") [25,40–43,45–48], in contrast to all the experiments, which

[*]billatkinson@trentu.ca

[†]arno.kampf@physik.uni-augsburg.de

find axial order. This discrepancy is resolved by imposing a pseudogap, from which charge order emerges [26,39,49,50]. This is not a unique resolution, though: some authors pointed out that axial and diagonal instabilities are close competitors [44,51], and in Ref. [52] the inclusion of Aslamazov-Larkin vertex corrections led to axial order. Empirically, however, it does appear that the pseudogap is a prerequisite for the formation of the dCDW in hole-doped cuprates, since T_{co} is always less than or equal to T^*. While the underlying reason is unclear, it is possible that short quasiparticle lifetimes at temperatures $T > T^*$ inhibit the formation of charge order [53].

If a correct description of the dCDW requires a basic understanding of the pseudogap phase, then it is disheartening that the cause of the pseudogap is still unknown. Many recent proposals suggest that the pseudogap is the result of fluctuations of, or competition between, multiple distinct order parameters [54–58] involving charge and superconductivity. Alternatively, dynamical mean-field calculations find that in the strongly correlated limit, local Coulomb interactions may generate a spectral pseudogap without need for a true phase transition; this is linked to dynamical antiferromagnetic correlations [59,60]. However, there is experimental evidence for a true thermodynamic phase transition [61,62] at T^* (although this has been challenged in Ref. [63]) that terminates at a quantum critical point near $p = 0.19$ [64–67]. One prominent suggestion is that the phase below T^* breaks time-reversal symmetry via microscopic loop currents (LCs) that may [68–72] or may not [65] break the translational symmetry of the lattice.

Considerations about the relationship between the dCDW and the pseudogap recently led us to reexamine the instabilities of multiorbital models for cuprate superconductors [73]. For physically relevant model parameters, we found a leading instability towards a spontaneous π-loop-current (πLC) phase, in which the circulation of the loop currents alternates to form an orbital antiferromagnet, similar to staggered LC phases that have been proposed in the past [68–72]. While direct experimental evidence for staggered LC phases in cuprates is still lacking [74–78], we are nonetheless motivated to study the LC phase for two reasons: first, the persistence with which LC phases are predicted by theory makes it plausible that there exist systems in which LCs are of key importance; second, phase competition of the type found in the cuprates can lead to emergent properties that are distinct from those of the constituent phases.

Here, our starting point is the assumption that the pseudogap follows from a πLC phase, and we focus on the possible emergence of charge order within this phase. The required formalism is developed in Sec. II, and results thereby obtained are presented in Sec. III. We show in Sec. III A that the encountered phases originate from different interactions: the πLC phase is driven primarily by the Coulomb repulsion between nearest-neighbor copper and oxygen orbitals, while charge ordering is driven by oxygen-oxygen repulsion. In Sec. III B we discuss that axial dCDWs can emerge within the πLC phase while diagonal dCDWs are strongly suppressed. In some cases we find a wide temperature range below the πLC transition and above the axial dCDW transition, over which the susceptibility towards an axial dCDW is large.

In these cases, short-range charge order may be induced by doping-related disorder. One important consequence relates to the Kerr effect that has been measured in YBa$_2$Cu$_3$O$_{6+x}$ [79,80]; a nonzero signal implies that both time-reversal and mirror symmetries are broken. The spontaneous currents in the πLC phase break time-reversal symmetry, and mirror symmetries are further broken with the development of the dCDW phase. The coexistence of loop currents and dCDW order therefore offers a candidate case for the observed Kerr rotation.

II. CALCULATIONS

A. Hamiltonian

We adopt a three-band model for the CuO$_2$ primitive unit cell, as described in Ref. [25]. The model includes the Cu$d_{x^2-y^2}$ orbital and the Op orbital from each oxygen that forms a σ bond with it; we label these Op_x and Op_y. The noninteracting part of the Hamiltonian is

$$\hat{H}_0 = \sum_{\mathbf{k},\sigma} \sum_{\alpha,\beta} c^\dagger_{\mathbf{k}\alpha\sigma} h_{0,\alpha\beta}(\mathbf{k}) c_{\mathbf{k}\beta\sigma}, \qquad (1)$$

where σ is a spin index and α,β denote the orbitals. We take the convention that $c_{\mathbf{k}\beta\sigma}$ is an *electron* annihilation operator. Because the πLC phase has a periodicity of two unit cells, we use a supercell comprising two primitive CuO$_2$ unit cells so that orbital labels run from 1 to 6 (Fig. 1).

We assume that the SU(2) spin invariance is unbroken so that spin-up and spin-down electrons satisfy identical equations of motion. For brevity, we therefore suppress the spin index except where it is required.

The Hamiltonian has diagonal matrix elements $h_{0,\alpha\alpha}(\mathbf{k})$ given by the on-site energies ϵ_d (for $\alpha = 1,4$) and ϵ_p (otherwise). The model further includes nearest-neighbor hopping between Cu and O orbitals with amplitude t_{pd}, and between adjacent O orbitals with amplitude t_{pp}. The Hamiltonian
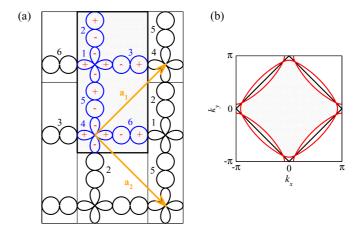

FIG. 1. Unit supercell and Brillouin zone. (a) The supercell (shaded region) contains two CuO$_2$ primitive unit cells, with orbitals numbered 1 through 6 as shown. The plus and minus signs indicate the sign convention for the lobes of the Cu$d_{x^2-y^2}$, Op_x, and Op_y orbitals. The lattice vectors $\mathbf{a}_1$ and $\mathbf{a}_2$ lead to the folded Brillouin zone shown in (b) (shaded region). Backfolded Fermi surfaces are shown for hole filling $p = 0.15$ (thick red lines).

matrix in Eq. (1) is therefore

$$\mathbf{h}_0(\mathbf{k}) = \begin{bmatrix} \mathbf{h}_1(\mathbf{k}) & \mathbf{h}_2(\mathbf{k}) \\ \mathbf{h}_2(\mathbf{k})^\dagger & \mathbf{h}_1(\mathbf{k}) \end{bmatrix}, \qquad (2)$$

where

$$\mathbf{h}_1(\mathbf{k}) = \begin{bmatrix} \epsilon_d & t_{pd}e^{ik_y/2} & -t_{pd}e^{ik_x/2} \\ t_{pd}e^{-ik_y/2} & \epsilon_p & 2t_{pp}c_- \\ -t_{pd}e^{-ik_x/2} & 2t_{pp}c_- & \epsilon_p \end{bmatrix}, \quad (3)$$

$$\mathbf{h}_2(\mathbf{k}) = \begin{bmatrix} 0 & -t_{pd}e^{-ik_y/2} & t_{pd}e^{-ik_x/2} \\ -t_{pd}e^{ik_y/2} & 0 & -2t_{pp}c_+ \\ t_{pd}e^{ik_x/2} & -2t_{pp}c_+ & 0 \end{bmatrix}. \quad (4)$$

The primitive lattice constant is $a_0 = 1$, and $c_\pm = \cos(\frac{k_x}{2} \pm \frac{k_y}{2})$. The signs of the off-diagonal matrix elements $h_{0,\alpha\beta}(\mathbf{k})$ are determined by the product of signs of the closest lobes of orbitals α and β, as shown in Fig. 1(a). Because the supercell contains two primitive unit cells, the Brillouin zone is halved and the Fermi surface is folded into the reduced Brillouin zone [Fig. 1(b)].

We consider both on-site and nearest-neighbor Coulomb repulsion, so the interaction has the form

$$\hat{V} = \sum_{i\alpha} U_\alpha \hat{n}_{i\alpha\uparrow}\hat{n}_{i\alpha\downarrow} + \frac{1}{2}\sum_{i\alpha\sigma, j\beta\sigma'} V_{i\alpha, j\beta}\hat{n}_{i\alpha\sigma}\hat{n}_{j\beta\sigma'}, \quad (5)$$

where i and j label supercells, α and β label orbitals, σ and σ' label spins, and $\hat{n}_{i\alpha\sigma} = c^\dagger_{i\alpha\sigma}c_{i\alpha\sigma}$. The on-site Coulomb interaction U_α is U_d ($\alpha = 1, 4$) or U_p (otherwise); the nonlocal interaction $V_{i\alpha, j\beta}$ is V_{pd} for nearest-neighbor p and d orbitals, and V_{pp} for adjacent oxygen orbitals.

Values for the model parameters based on density functional theory (DFT) are given, for example, in Ref. [81]. While these parameters correctly predict the shape of the observed Fermi surface, DFT overestimates the Fermi velocities by a factor of 2–4 (see, e.g., Ref. [82]): based on the dispersion obtained numerically from the parameters given below, the nodal Fermi velocity of our model is $v_F = 4.7t_{pd}$; this reproduces the experimental values $v_F \sim 1$–2 eV Å (depending on doping) [83] provided $t_{pd} \sim 0.2$–0.5 eV; for comparison, Hybertsen *et al.* [81] suggest $t_{pd} = 1.3$ eV. To keep the discussion general, we adopt dimensionless parameters in which the unit of energy is set to $t_{pd} = 1$; in units of t_{pd}, we take $t_{pp} = -0.5$ and $\epsilon_d - \epsilon_p = 2.5$. These values give a Fermi surface consistent with experiments.

The interaction strengths are $U_d = 9.0, U_p = 3.0$, while V_{pp} and V_{pd} are varied in the ranges 1.0–1.3 and 2.0–3.0, respectively. The most important interactions in our calculations are V_{pd} and V_{pp}, as these drive the loop-current and charge-ordering transitions, respectively. Typical calculations [81] take $V_{pd} \sim 1$ eV, while V_{pp} is not well known, with most authors neglecting it. The comparatively large value of t_{pp} that emerges from DFT, however, suggests a sizable overlap between adjacent Op orbitals such that V_{pp} is nonvanishing. In this work, we find that even a comparatively small value of V_{pp} may drive charge instabilities consistent with those observed experimentally.

We treat the interactions within a mean-field Hartree-Fock approximation. The principal weakness of this approach is that it neglects strong correlations due to the local Coulomb

interaction on the Cu sites. These strong correlations renormalize the dynamics of doped holes in underdoped cuprates, and generate an effective low-energy spin-exchange interaction between nearest-neighbor sites [84]. Empirically, the cuprates' underlying Fermi surface is quantitatively similar to that predicted by band structure calculations [85], albeit with renormalized bandwidths, and the principal assumption of our calculation is that strong correlation effects can be absorbed into renormalized model parameters, as discussed above. The spin-exchange interaction certainly contributes to charge order, and it has been extensively studied in the context of one-band spin-fermion models [40–44]. Our neglect of the spin-exchange interaction here makes our discussion qualitative, rather than quantitative. Rather, our focus on short-range Coulomb interactions allows us to identify routes to broken-symmetry phases that have been previously neglected, and in particular to focus on intra-unit-cell degrees of freedom. Unlike U_d, V_{pd} and V_{pp} (which are responsible for the main results of this work) are comparatively weak relative to the bandwidth, and we therefore expect that their main qualitative effects can be captured within weak-coupling approaches.

Of the methods to deal explicitly with strong correlations, dynamical mean-field theory (DMFT), has been most successfully applied to broken-symmetry phases in cuprates [86–88]. While the physics of U_d can be accounted for by DMFT methods, nonlocal interactions in particular between electrons in orbitals of adjacent unit cells require further approximations. A particular challenge for DMFT calculations is that they lack the resolution in momentum space required to realize an incommensurate CDW phase.

B. Hartree-Fock approximation

Interactions are first treated within a Hartree-Fock (HF) approximation, $\hat{V} \approx \hat{V}_{\text{HF}} \equiv \hat{V}_H + \hat{V}_X$, where the Hartree term is

$$\hat{V}_H = \sum_{i\alpha\sigma} U_\alpha \hat{n}_{i\alpha\sigma}n_{i\alpha\overline{\sigma}} + \sum_{i\alpha\sigma, j\beta\sigma'} V_{i\alpha, j\beta}\hat{n}_{i\alpha\sigma}n_{j\beta\sigma'}, \quad (6)$$

with $\overline{\sigma} \equiv -\sigma$ and $n_{i\alpha\sigma} \equiv \langle\hat{n}_{i\alpha\sigma}\rangle$, and the exchange term is

$$\hat{V}_X = -\sum_{i\alpha, j\beta}\sum_\sigma c^\dagger_{i\alpha\sigma}c_{j\beta\sigma} V_{i\alpha, j\beta}\langle c^\dagger_{j\beta\sigma}c_{i\alpha\sigma}\rangle. \quad (7)$$

Within the HF approximation, the leading instability is to a spin-density-wave (SDW) state involving spins on the Cu sites [25]. This state is driven by the large local Coulomb interaction U_d; it is well known that strong correlations suppress the SDW except near half filling, and we therefore make a restricted HF approximation that preserves the SU(2) invariance of the spins. SU(2) symmetry implies $n_{i\alpha\uparrow} = n_{i\alpha\downarrow}$ and $\langle c^\dagger_{j\beta\uparrow}c_{i\alpha\uparrow}\rangle = \langle c^\dagger_{j\beta\downarrow}c_{i\alpha\downarrow}\rangle$, so that the HF Hamiltonian is identical for spin-up and spin-down electrons.

Expressing $\hat{V}_{\text{HF}}$ in terms of Bloch states (and suppressing the spin index) gives

$$\hat{V}_{\text{HF}} = \sum_{\mathbf{k},\mathbf{q},\alpha,\beta} P_{\alpha\beta}(\mathbf{k},\mathbf{q})c^\dagger_{\mathbf{k}+\frac{\mathbf{q}}{2}\alpha}c_{\mathbf{k}-\frac{\mathbf{q}}{2}\beta}, \quad (8)$$

where

$$P_{\alpha\beta}(\mathbf{k},\mathbf{q}) = \frac{1}{N}\sum_{\mathbf{k}'}\sum_{\mu,\nu}\{[U_\alpha\delta_{\alpha,\mu} + 2V_{\alpha\mu}(\mathbf{q})]\delta_{\alpha,\beta}\delta_{\mu,\nu}$$
$$- V_{\alpha\beta}(\mathbf{k}-\mathbf{k}')\delta_{\nu,\beta}\delta_{\mu,\alpha}\}\langle c_{\mathbf{k}'-\frac{\mathbf{q}}{2}\nu}^\dagger c_{\mathbf{k}'+\frac{\mathbf{q}}{2}\mu}\rangle \quad (9)$$

is the HF "self-energy" and

$$V_{\alpha\beta}(\mathbf{q}) = \sum_{\mathbf{r}_{\alpha\beta}} e^{i\mathbf{q}\cdot\mathbf{r}_{\alpha\beta}} V_{\alpha\beta}(\mathbf{r}_{\alpha\beta}), \quad (10)$$

with $\{\mathbf{r}_{\alpha\beta}\}$ the set of intra- and inter-supercell vectors pointing *from* orbital α *to* nearest-neighbor orbital β. Explicit expressions for $V_{\alpha\beta}(\mathbf{q})$ are given in Appendix A.

In the HF approximation, terms proportional to U_α contribute only Hartree terms, while the nonlocal terms make both Hartree and exchange contributions. Because our model parameters are chosen phenomenologically to reproduce the cuprate band structure, the homogeneous components of the Hartree and exchange self-energies are implicitly present in the site energies ϵ_d and ϵ_p and hopping matrix elements t_{pd} and t_{pp}. To avoid double counting, we retain only the spatially inhomogeneous components of the interaction self-energy; these will prove responsible for both loop currents and charge order.

It is convenient to decompose the interactions in Eq. (9) in a set of basis functions $g_{\alpha\beta}^\ell(\mathbf{k})$:

$$[U_\alpha\delta_{\alpha,\mu} + 2V_{\alpha\mu}(\mathbf{q})]\delta_{\alpha,\beta}\delta_{\mu,\nu} - V_{\alpha\beta}(\mathbf{k}-\mathbf{k}')\delta_{\nu,\beta}\delta_{\mu,\alpha}$$
$$= \sum_{\ell,\ell'}\tilde{V}^{\ell\ell'}(\mathbf{q})g_{\alpha\beta}^\ell(\mathbf{k})g_{\mu\nu}^{\ell'}(\mathbf{k}')^*. \quad (11)$$

Here $g_{\alpha\beta}^\ell(\mathbf{k})$ are 6×6 matrices in the orbital indices α and β, with a single nonzero matrix element corresponding to a unique bond or site:

$$g_{\alpha\beta}^\ell(\mathbf{k}) = e^{i\mathbf{k}\cdot\mathbf{r}_{\alpha\beta}}\delta_{\alpha,\alpha_\ell}\delta_{\beta,\beta_\ell}, \quad (12)$$

where each ℓ labels either a directed bond pointing from α_ℓ to β_ℓ, or an orbital when $\alpha_\ell = \beta_\ell$. There are a total of 38 orbital pairs (α_ℓ,β_ℓ), and these are listed in Table I, along with the corresponding basis functions. Here, we note that $\ell\in[1,32]$ labels the directed bonds between nearest-neighbor sites, and $\ell\in[33,38]$ labels the six orbitals making up the supercell.

With the decomposition (11), we obtain

$$P_{\alpha\beta}(\mathbf{k},\mathbf{q}) = \sum_\ell \tilde{P}^\ell(\mathbf{q})g_{\alpha\beta}^\ell(\mathbf{k}), \quad (13)$$

where

$$\tilde{P}^\ell(\mathbf{q}) = \frac{1}{N}\sum_{\mathbf{k}'}\sum_{\ell',\mu,\nu}\tilde{V}^{\ell\ell'}(\mathbf{q})g_{\mu\nu}^{\ell'}(\mathbf{k}')^*\langle c_{\mathbf{k}'-\frac{\mathbf{q}}{2}\nu}^\dagger c_{\mathbf{k}'+\frac{\mathbf{q}}{2}\mu}\rangle \quad (14)$$

is the self-consistency equation for the HF self-energy for bond ℓ. To perform an unbiased search for broken-symmetry phases within HF theory, it is most convenient to linearize Eq. (14) so that it acquires the form

$$\tilde{P}^\ell(\mathbf{q}) = -\sum_{\ell',\ell''}\tilde{V}^{\ell\ell'}(\mathbf{q})\tilde{X}_0^{\ell'\ell''}(\mathbf{q})\tilde{P}^{\ell''}(\mathbf{q}). \quad (15)$$

This step is performed explicitly in the next section.

C. Linearized Hartree-Fock equations

We define a generalized susceptibility that describes the change in $\tilde{P}^\ell(\mathbf{q})$ induced by a perturbing field $\tilde{\phi}^{\ell'}(\mathbf{q},t)$, where ℓ and ℓ' label either bonds or sites as described above. In the limit of a vanishingly weak perturbation, a phase transition is signalled by a diverging susceptibility eigenvalue.

The general form of the perturbation is

$$\hat{\Phi}(t) = \sum_{m\mu,n\nu}\phi_{m\mu,n\nu}(t)c_{m\mu}^\dagger c_{n\nu}$$
$$= \sum_{\mathbf{k},\mathbf{q}}\sum_{\mu\nu}\phi_{\mu\nu}(\mathbf{k},\mathbf{q},t)c_{\mathbf{k}+\frac{\mathbf{q}}{2}\mu}^\dagger c_{\mathbf{k}-\frac{\mathbf{q}}{2}\nu}, \quad (16)$$

where m,n label supercells and

$$\phi_{\mu\nu}(\mathbf{k},\mathbf{q},t) = \frac{1}{N}\sum_{m,n}\phi_{m\mu,n\nu}(t)e^{i\mathbf{k}\cdot(\mathbf{r}_{n\nu}-\mathbf{r}_{m\mu})}e^{-i\frac{\mathbf{q}}{2}\cdot(\mathbf{r}_{m\mu}+\mathbf{r}_{n\nu})}. \quad (17)$$

In this equation, $\mathbf{k}$ is associated with the relative coordinate connecting orbitals μ and ν, while $\mathbf{q}$ is associated with the spatial modulation of the field; a conventional electrostatic potential would have

$$\phi_{\mu\nu}(\mathbf{k},\mathbf{q},t) = \delta_{\mu,\nu}\phi_\mu(\mathbf{q},t). \quad (18)$$

Provided the perturbation is restricted to on-site and nearest-neighbor terms, Eq. (17) can be decomposed in terms of

TABLE I. The basis functions $g_{\alpha\beta}^\ell(\mathbf{k}) = g^\ell(\mathbf{k})\delta_{\alpha,\alpha_\ell}\delta_{\beta,\beta_\ell}$. The index ℓ labels the different basis functions, and each ℓ corresponds to a unique pair of orbitals α_ℓ and β_ℓ for which $g_{\alpha_\ell\beta_\ell}^\ell(\mathbf{k})$ is nonzero. In this basis, and for $\ell\in[1,32]$, the quantity $\tilde{P}^\ell$ defined in Eq. (14) is simply the bond self-energy $P_{i\alpha,j\beta}$ for nearest-neighbor sites $i\alpha,j\beta$. For $\ell\in[17,32]$, there are two nearest-neighbor pairs for each α,β, and to remove the ambiguity, the table shows the vector $\mathbf{r}_{\alpha\to\beta}$ pointing from α to β. The basis functions with $\ell\in[33,38]$ are used to represent the Hartree self-energies.

ℓ	α_ℓ	β_ℓ	$g^\ell(\mathbf{k})$	ℓ	α_ℓ	β_ℓ	$g^\ell(\mathbf{k})$	ℓ	α_ℓ	β_ℓ	$g^\ell(\mathbf{k})$	$\mathbf{r}_{\alpha\to\beta}$	ℓ	α_ℓ	β_ℓ	$g^\ell(\mathbf{k})$	$\mathbf{r}_{\alpha\to\beta}$	ℓ	α_ℓ	β_ℓ	$g^\ell(\mathbf{k})$
1	1	2	$e^{ik_y/2}$	9	2	1	$e^{-ik_y/2}$	17	2	3	$e^{i(k_x-k_y)/2}$	$+\mathbf{a}_2/2$	25	3	2	$e^{-i(k_x-k_y)/2}$	$-\mathbf{a}_2/2$	33	1	1	1
2	1	3	$e^{ik_x/2}$	10	3	1	$e^{-ik_x/2}$	18	2	3	$e^{-i(k_x-k_y)/2}$	$-\mathbf{a}_2/2$	26	3	2	$e^{i(k_x-k_y)/2}$	$+\mathbf{a}_2/2$	34	2	2	1
3	1	5	$e^{-ik_y/2}$	11	5	1	$e^{ik_y/2}$	19	2	6	$e^{i(k_x+k_y)/2}$	$+\mathbf{a}_1/2$	27	6	2	$e^{-i(k_x+k_y)/2}$	$-\mathbf{a}_1/2$	35	3	3	1
4	1	6	$e^{-ik_x/2}$	12	6	1	$e^{ik_x/2}$	20	2	6	$e^{-i(k_x+k_y)/2}$	$-\mathbf{a}_1/2$	28	6	2	$e^{i(k_x+k_y)/2}$	$+\mathbf{a}_1/2$	36	4	4	1
5	4	5	$e^{ik_y/2}$	13	5	4	$e^{-ik_y/2}$	21	5	6	$e^{i(k_x-k_y)/2}$	$+\mathbf{a}_2/2$	29	6	5	$e^{-i(k_x-k_y)/2}$	$-\mathbf{a}_2/2$	37	5	5	1
6	4	6	$e^{ik_x/2}$	14	6	4	$e^{-ik_x/2}$	22	5	6	$e^{-i(k_x-k_y)/2}$	$-\mathbf{a}_2/2$	30	6	5	$e^{i(k_x-k_y)/2}$	$+\mathbf{a}_2/2$	38	6	6	1
7	4	2	$e^{-ik_y/2}$	15	2	4	$e^{ik_y/2}$	23	3	5	$e^{i(k_x+k_y)/2}$	$+\mathbf{a}_1/2$	31	5	3	$e^{-i(k_x+k_y)/2}$	$-\mathbf{a}_1/2$				
8	4	3	$e^{-ik_x/2}$	16	3	4	$e^{ik_x/2}$	24	3	5	$e^{-i(k_x+k_y)/2}$	$-\mathbf{a}_1/2$	32	5	3	$e^{i(k_x+k_y)/2}$	$+\mathbf{a}_1/2$				

$g^\ell_{\mu\nu}(\mathbf{k})$,

$$\phi_{\mu\nu}(\mathbf{k},\mathbf{q},t) = \sum_\ell \tilde{\phi}^\ell(\mathbf{q},t) g^\ell_{\mu\nu}(\mathbf{k}). \qquad (19)$$

Then

$$\hat{\Phi}(t) = \sum_{\mathbf{k},\mathbf{q}} \sum_{\mu\nu} \sum_\ell \tilde{\phi}^\ell(\mathbf{q},t) g^\ell_{\mu\nu}(\mathbf{k}) c^\dagger_{\mathbf{k}+\frac{\mathbf{q}}{2}\mu} c_{\mathbf{k}-\frac{\mathbf{q}}{2}\nu}. \qquad (20)$$

Hermiticity of $\hat{\Phi}(t)$ requires for the perturbing fields

$$\tilde{\phi}^\ell(-\mathbf{q},t) = \tilde{\phi}^{\bar{\ell}}(\mathbf{q},t)^*, \qquad (21)$$

where ℓ and $\bar{\ell}$ describe the same bond, but oriented in opposite directions.

The perturbing field induces time-dependent collective excitations $\delta P_{\alpha\beta}(\mathbf{k},\mathbf{q},t)$ of the self-energy $P_{\alpha\beta}(\mathbf{k},\mathbf{q})$; these feed back into the linear response, so that the total perturbation is

$$\hat{H}'(t) = \sum_{\mathbf{q}} \sum_\ell [\delta\tilde{P}^\ell(\mathbf{q},t) + \tilde{\phi}^\ell(\mathbf{q},t)]$$
$$\times \sum_{\mathbf{k}\mu\nu} g^\ell_{\mu\nu}(\mathbf{k}) c^\dagger_{\mathbf{k}+\frac{\mathbf{q}}{2}\mu} c_{\mathbf{k}-\frac{\mathbf{q}}{2}\nu}, \qquad (22)$$

where we have expanded $\delta P_{\mu\nu}(\mathbf{k},\mathbf{q},t) = \sum_\ell g^\ell_{\mu\nu}(\mathbf{k})\delta\tilde{P}^\ell(\mathbf{q},t)$.

A self-consistent expression for $\delta\tilde{P}^\ell(\mathbf{q},t)$ is obtained from Kubo's equation for the first-order response of the charge density to $\hat{H}'(t)$:

$$\delta\tilde{P}^\ell(\mathbf{q},t) = -i \int_{-\infty}^t dt' \langle [\hat{P}^\ell(\mathbf{q},t),\hat{H}'(t')] \rangle, \qquad (23)$$

where

$$\hat{P}^\ell(\mathbf{q}) = \frac{1}{N} \sum_{\mathbf{k}'} \sum_{\ell',\mu,\nu} \tilde{V}^{\ell\ell'}(\mathbf{q}) g^{\ell'}_{\mu\nu}(\mathbf{k}')^* c^\dagger_{\mathbf{k}'-\frac{\mathbf{q}}{2}\nu} c_{\mathbf{k}'+\frac{\mathbf{q}}{2}\mu} \qquad (24)$$

is the operator form of $\tilde{P}^\ell(\mathbf{q})$ [see Eq. (14)]. A straightforward calculation yields

$$\delta\tilde{\mathbf{P}}(\mathbf{q},\omega) = -\tilde{\mathbf{V}}(\mathbf{q})\tilde{\mathbf{X}}_0(\mathbf{q},\omega)[\delta\tilde{\mathbf{P}}(\mathbf{q},\omega) + \tilde{\boldsymbol{\phi}}(\mathbf{q},\omega)], \qquad (25)$$

where bold symbols represent matrices and vectors in the 38×38 bond and orbital basis. The bare susceptibility matrix has elements

$$\tilde{X}_0^{\ell\ell'}(\mathbf{q},\omega) = \frac{1}{N} \sum_{\mathbf{k}} \sum_{\alpha\beta\mu\nu} g^\ell_{\mu\nu}(\mathbf{k})^* g^{\ell'}_{\alpha\beta}(\mathbf{k})$$
$$\times \sum_{n,n'} \Psi_{\mu n}(\mathbf{k}_+)\Psi^*_{\alpha n}(\mathbf{k}_+)\Psi_{\beta n'}(\mathbf{k}_-)\Psi^*_{\nu n'}(\mathbf{k}_-)$$
$$\times \frac{f(E_{n\mathbf{k}_+}) - f(E_{n'\mathbf{k}_-})}{\omega + i\delta - E_{n\mathbf{k}_+} + E_{n'\mathbf{k}_-}}, \qquad (26)$$

where $\mathbf{k}_\pm \equiv \mathbf{k} \pm \frac{\mathbf{q}}{2}$, Greek symbols are orbital labels, n and n' are band indices, and $E_{n\mathbf{k}}$ and $\Psi_{\mu n}(\mathbf{k})$ are respectively the eigenvalues and eigenvectors of the Hamiltonian $\hat{H}_0$. In the static limit $\omega \to 0$ and for a vanishingly weak external potential $\tilde{\phi}^\ell(\mathbf{q},\omega)$, Eq. (25) reduces to Eq. (15).

Equation (25) is a 38×38 matrix equation that can be inverted for each $\mathbf{q}$ and ω to obtain

$$\delta\tilde{\mathbf{P}}(\mathbf{q},\omega) = -\tilde{\mathbf{V}}(\mathbf{q})\tilde{\mathbf{X}}(\mathbf{q},\omega)\tilde{\boldsymbol{\phi}}(\mathbf{q},\omega) \qquad (27)$$

with

$$\tilde{\mathbf{X}}(\mathbf{q},\omega) = [\mathbf{1} + \tilde{\mathbf{X}}_0(\mathbf{q},\omega)\tilde{\mathbf{V}}(\mathbf{q})]^{-1}\tilde{\mathbf{X}}_0(\mathbf{q},\omega). \qquad (28)$$

Equation (27) describes the change in the HF self-energy induced by a weak perturbing field.

D. Connection to charge and current densities

We denote by $\chi(\mathbf{q})$ the largest eigenvalue of the static susceptibility matrix $\tilde{\mathbf{X}}(\mathbf{q},0)$. The divergence of $\chi(\mathbf{q})$ as temperature is lowered signals a phase transition. Further information about the resulting phase is obtained from the corresponding eigenvector $\tilde{\mathbf{v}}_\mathbf{q}$. In particular, both the current and charge density can be obtained from a generalized charge density,

$$\rho_{i\alpha,j\beta} = \langle c^\dagger_{i\alpha} c_{j\beta} \rangle, \qquad (29)$$

which is closely related to the HF self-energy by

$$P_{i\alpha,j\beta} = V_{i\alpha,j\beta}\rho^*_{i\alpha,j\beta}. \qquad (30)$$

For $(i\alpha) = (j\beta)$, $\rho_{i\alpha,j\beta}$ reduces to the single-spin charge density $n_{i\alpha}$, while for nearest-neighbor pairs $(i\alpha)$ and $(j\beta)$, the imaginary part of $\rho_{i\alpha,j\beta}$ gives the probability current along the bond from $(i\alpha)$ to $(j\beta)$,

$$J_{i\alpha,j\beta} = -2t_{i\alpha,j\beta}\text{Im}[\rho_{i\alpha,j\beta}]. \qquad (31)$$

In Eq. (31), $t_{i\alpha,j\beta}$ is $\pm t_{pd}$ or $\pm t_{pp}$, depending on the bond type, where the sign depends on the relative signs of the closest lobes of orbitals α and β in Fig. 1 (thus $t_{i1,i3} = -t_{pd}$; $t_{i5,i6} = +t_{pp}$).

By Fourier-transforming Eq. (30) and expanding left and right sides in terms of the basis functions $g^\ell_{\alpha\beta}(\mathbf{k})$, we obtain

$$\tilde{P}^\ell(\mathbf{q}) = \sum_{\ell'} \tilde{V}^{\ell\ell'}\tilde{\rho}^{\ell'}(-\mathbf{q})^*, \qquad (32)$$

with

$$\tilde{\rho}^{\ell'}(\mathbf{q}) = \frac{1}{N} \sum_{\mathbf{k},\alpha,\beta} g^\ell_{\alpha\beta}(\mathbf{k}) \langle c^\dagger_{\mathbf{k}-\frac{\mathbf{q}}{2}\alpha} c_{\mathbf{k}+\frac{\mathbf{q}}{2}\beta} \rangle. \qquad (33)$$

Equation (32) provides a connection between the induced self-energy $\delta\tilde{\mathbf{P}}(\mathbf{q},\omega)$ in Eq. (27) and the corresponding induced change in the generalized charge density $\delta\tilde{\boldsymbol{\rho}}(\mathbf{q},\omega)$.

Near the phase transition, the static susceptibility matrix $\tilde{\mathbf{X}}(\mathbf{q})$ is dominated by the diverging eigenvalue $\chi(\mathbf{q})$, such that

$$\tilde{\mathbf{X}}(\mathbf{q}) \approx \chi(\mathbf{q})\tilde{\mathbf{v}}_\mathbf{q}\tilde{\mathbf{v}}^\dagger_\mathbf{q}, \qquad (34)$$

where $\tilde{\mathbf{v}}_\mathbf{q}$ is the column eigenvector corresponding to $\chi(\mathbf{q})$, $\tilde{\mathbf{v}}^\dagger_\mathbf{q}$ is the transpose conjugate, and the outer product $\tilde{\mathbf{v}}_\mathbf{q}\tilde{\mathbf{v}}^\dagger_\mathbf{q}$ generates a matrix. Substitution of Eq. (32) into Eq. (27) immediately yields the induced static (generalized) charge density,

$$\delta\tilde{\boldsymbol{\rho}}(-\mathbf{q})^* = -\tilde{\mathbf{X}}(\mathbf{q})\tilde{\boldsymbol{\phi}}(\mathbf{q})$$
$$= -\varphi_\mathbf{q}\chi(\mathbf{q})\tilde{\mathbf{v}}_\mathbf{q}, \qquad (35)$$

where $\varphi_\mathbf{q} = \tilde{\mathbf{v}}^\dagger_\mathbf{q} \cdot \tilde{\boldsymbol{\phi}}(\mathbf{q})$ is the projection of the field onto the diverging eigenmode. The Hermiticity condition (21), along with a similar condition for $\tilde{\mathbf{v}}_\mathbf{q}$ [see Eq. (B9) in Appendix B],

imposes the constraint $\varphi_{-\mathbf{q}} = \varphi_{\mathbf{q}}$. Then,

$$\delta\rho_{i\alpha,j\beta} = \delta\rho(\mathbf{q})e^{i\frac{\mathbf{q}}{2}\cdot(\mathbf{r}_{i\alpha}+\mathbf{r}_{j\beta})} + \delta\rho(-\mathbf{q})e^{-i\frac{\mathbf{q}}{2}\cdot(\mathbf{r}_{i\alpha}+\mathbf{r}_{j\beta})}$$

$$= -\chi(\mathbf{q})\{e^{i\frac{\mathbf{q}}{2}\cdot(\mathbf{r}_{i\alpha}+\mathbf{r}_{j\beta})}\varphi_{\mathbf{q}}\tilde{v}_{\mathbf{q}}^{\bar{\ell}} + e^{-i\frac{\mathbf{q}}{2}\cdot(\mathbf{r}_{i\alpha}+\mathbf{r}_{j\beta})}\varphi_{\mathbf{q}}^*\tilde{v}_{\mathbf{q}}^{\ell*}\}, \quad (36)$$

where ℓ denotes the directed bond from $(i\alpha)$ to $(j\beta)$, and $\bar{\ell}$ denotes the oppositely directed bond. The complex phase of $\phi_{\mathbf{q}}$ shifts the density wave spatially, and can therefore be set to zero without loss of generality:

$$\delta\rho_{i\alpha,j\beta} = -\chi(\mathbf{q})\varphi_{\mathbf{q}}\{e^{i\frac{\mathbf{q}}{2}\cdot(\mathbf{r}_{i\alpha}+\mathbf{r}_{j\beta})}\tilde{v}_{\mathbf{q}}^{\bar{\ell}} + e^{-i\frac{\mathbf{q}}{2}\cdot(\mathbf{r}_{i\alpha}+\mathbf{r}_{j\beta})}\tilde{v}_{\mathbf{q}}^{\ell*}\}. \quad (37)$$

Real-space patterns shown in the next section are calculated from the portion of Eq. (37) contained in braces.

III. RESULTS

A. Instabilities of the normal state

As there are no broken symmetries in the normal high-temperature phase, the HF self-energy generates only a homogeneous renormalization of the model parameters. As discussed above, this homogeneous component is absorbed into the phenomenological model parameters to avoid double counting. We therefore construct the generalized static susceptibility $\tilde{\mathbf{X}}(\mathbf{q})$ from the eigenstates of the bare Hamiltonian $\hat{H}_0$, defined in Eq. (1).

Figure 2 shows the largest eigenvalue $\chi(\mathbf{q})$ of $\tilde{\mathbf{X}}(\mathbf{q})$ as a function of $\mathbf{q}$ close to an instability approached upon cooling. The generalized charge susceptibility allows transitions to charge-, bond-, and current-ordered phases, and the multipeak structure in Fig. 2 indicates proximity to more than one distinct ordered phase. Because our supercell contains two primitive cells, the points $\mathbf{q} = (0,0)$ and $\mathbf{q} = (\pi,\pi)$ are equivalent. Furthermore, peaks at (q,q) and $(\pi-q,\pi-q)$ are related by symmetry. There are, therefore, only two distinct peaks in $\chi(\mathbf{q})$, corresponding to two distinct phases. We use the notation $\mathbf{q}_0 = (0,0)$ and $\mathbf{q}_1 = (q_1,q_1)$ to denote these two kinds of peaks, while $\mathbf{q}_2$ will be used later to denote peaks in the axial direction at $(q_2,0)$ or $(0,q_2)$.
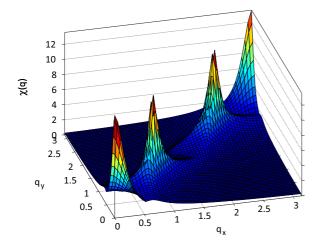

FIG. 2. Largest eigenvalue of the static susceptibility matrix $\tilde{\mathbf{X}}(\mathbf{q})$ in the normal state at $T = 0.010, V_{pd} = 2.5$, and $p = 0.10$. Throughout the paper, energies and temperatures are in units of t_{pd}.
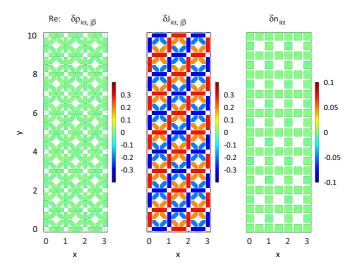

FIG. 3. Components of the induced generalized charge density $\delta\rho_{i\alpha,j\beta}$ associated with the $\mathbf{q}_0$ eigenmode for the susceptibility shown in Fig. 2. Real part of $\delta\rho_{i\alpha,j\beta}$ for $\alpha \neq \beta$ (left), induced currents $\delta J_{i\alpha,j\beta}$ (middle), and induced charge modulations $\delta n_{i\alpha}$ (right). Currents with a component of their flow in the positive x direction are deemed positive; currents flowing entirely along the y axis are positive in the positive y direction. $\delta\rho_{i\alpha,j\beta}$ is calculated from Eq. (37) with the prefactor $\chi(\mathbf{q})\varphi_{\mathbf{q}}$ set to 1; the color scale is therefore arbitrary.

For the chosen model parameters there are pronounced peaks at both $\mathbf{q}_0$ and $\mathbf{q}_1$. The peak at $\mathbf{q}_0$ diverges first as T is lowered, and is therefore the leading instability. To determine the nature of the instability, we construct the generalized charge density $\delta\rho_{i\alpha,j\beta}$ induced by an infinitesimally weak field using Eq. (37). The left panel of Fig. 3(a) shows the real part of $\delta\rho_{i\alpha,j\beta}$ for $\alpha \neq \beta$, which is related by Eq. (30) to the bond-strength renormalization. The imaginary parts of $\delta\rho_{i\alpha,j\beta}$ are proportional to the bond currents $\delta J_{i\alpha,j\beta}$, which are shown in the middle panel of Fig. 3(b), while the orbital charge modulations $\delta n_{i\alpha} = \delta\rho_{i\alpha,i\alpha}$ are shown in the right panel. From the figure, it is apparent that the $\mathbf{q}_0$ divergence corresponds to the onset of a staggered loop-current pattern, with no associated charge or bond order. [Note that $\mathbf{q}_0$ is a *supercell* wave vector, and that the current pattern has wave vector (π,π) in terms of the primitive unit cell.] This is the same πLC pattern that was identified previously in Ref. [73].

In contrast, Fig. 4 shows that the subdominant peak at $\mathbf{q}_1 = (0.84,0.84)$ corresponds to a diagonal dCDW with vanishing orbital currents. The period of this modulation is $2\pi/(0.84\sqrt{2}) = 5.3$ primitive unit cells, similar to what is found elsewhere, and agrees with the shortest wave vector which connects Fermi surface hot spots. This type of instability has been discussed at length in the literature [25,40–43,45–48].

While the details of the competition between the πLC and charge-ordered phases depend on the band structure, a simple picture emerges concerning the interactions driving these two phases. In Fig. 5 $\chi(\mathbf{q})$ is plotted along the Brillouin zone diagonal as functions of both V_{pd} and V_{pp}: Fig. 5(a) shows that $\chi(\mathbf{q}_0)$ is enhanced by increasing V_{pd} while Fig. 5(b) shows that $\chi(\mathbf{q}_1)$ is enhanced by increasing V_{pp}. This demonstrates that V_{pd} drives the πLC phase while V_{pp} drives the dCDW. The figure also shows that U_p weakens the charge-ordering
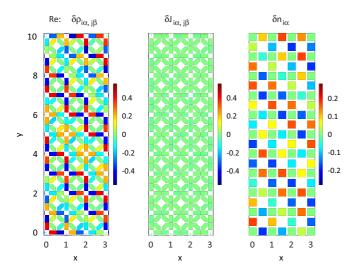
FIG. 4. As in Fig. 3, but for the peak in Fig. 2 at $\mathbf{q}_1 = (0.84, 0.84)$. This case corresponds to a diagonal dCDW with no circulating currents.

tendency, but has no effect on the πLC. We have further found that U_d affects neither the dCDW or the πLC peak.

Figures 6 and 7 show the dependence of the πLC phase on various model parameters. We caution that factors not included in our calculations must inevitably affect the phase diagram quantitatively. Notably, strong correlations renormalize the electronic effective mass, which grows as the hole doping p is reduced, and the enhanced spin fluctuations make a further doping-dependent contribution to the self-energy.

Figure 6 shows the phase diagram that follows from the susceptibility calculations within the symmetry-unbroken
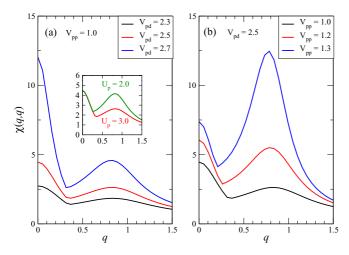

FIG. 5. Effects of V_{pd}, V_{pp}, and U_p on the susceptibility eigenvalue $\chi(\mathbf{q})$. Plots show cuts along the Brillouin zone diagonal, $\mathbf{q} = (q, q)$. Results are for (a) fixed $V_{pp} = 1.0$ and varying V_{pd}; (b) fixed $V_{pd} = 2.5$ and varying V_{pp}. V_{pd} enhances the loop-current susceptibility at $\mathbf{q}_0$, while V_{pp} enhances the charge susceptibility peak at $\mathbf{q}_1$. The inset shows that U_p opposes charge order but has no effect on the πLC susceptibility. U_d has no effect on either the πLC or the dCDW susceptibility (not shown). Results are for $T = 0.025$ (in units of t_{pd}) and hole density $p = 0.12$.
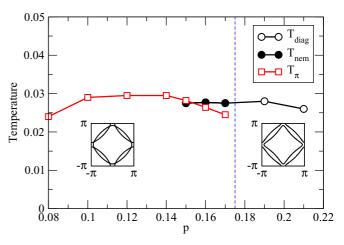

FIG. 6. Phase diagram of the three-band model from linear response theory. The figure shows the doping dependence of the leading instability temperature of the generalized susceptibility $\tilde{\mathbf{X}}(\mathbf{q})$. The Van Hove hole density p_{VH} is indicated by a vertical dashed line, and representative Fermi surfaces for $p < p_{\mathrm{VH}}$ and $p > p_{\mathrm{VH}}$ are shown in the insets. The leading instability is to a πLC for $p < 0.154$ and to a charge-ordered state for $p > 0.154$. There are two charge-ordered states shown: a diagonal dCDW below T_{diag} for $p < p_{\mathrm{VH}}$, and a nematic phase below T_{nem} for $p > p_{\mathrm{VH}}$. The nematic phase consists of a translationally invariant intra-unit-cell transfer of charge between adjacent oxygen orbitals [25]. Results are for $V_{pd} = 3.0, V_{pp} = 1.0$.

normal state. The Van Hove filling p_{VH} denotes the crossover from a hole-like Fermi surface at $p < p_{\mathrm{VH}}$ to an electron-like Fermi surface at $p > p_{\mathrm{VH}}$. For the parameter sets studied in this work, the πLC is restricted to the region $p < p_{\mathrm{VH}}$, while charge-ordering tendencies are found for both hole- and electron-like Fermi surfaces. It was found previously [25] that in the region $p < p_{\mathrm{VH}}$, the leading charge instability is to a
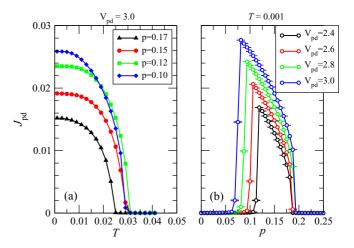

FIG. 7. Self-consistent Hartree-Fock results for the orbital current as a function of hole filling p, temperature T, and interaction V_{pd}. The current J_{pd} along the p-d bond is shown as a function of (a) T for $V_{pd} = 3.0$ and (b) p for various V_{pd} at $T = 0.001$. The ratio of the p-p and p-d bond currents is $J_{pp}/J_{pd} = 0.32$, independently of T, p, and V_{pd}. It was previously found to depend on the ratio of t_{pp}/t_{pd} [73]. The current is in units of $et_{pd}/\hbar$, with e the electron charge.

diagonal dCDW, while for $p > p_{VH}$ the tendency is towards either a $\mathbf{q} = (0,0)$ nematic phase with an intra-unit-cell charge redistribution or an axial dCDW. For the model parameters chosen in Fig. 6, there is a crossover from πLC to dCDW near $p = 0.154$, and a second crossover from dCDW to nematic at p_{VH}.

To better understand the phase diagram, we show in Fig. 7 the results of self-consistent HF calculations for the πLC phase, neglecting competition from charge order. For these calculations, the self-energy has the periodicity of the supercell, and Eq. (14) can be expressed simply in terms of the eigenvalues $E_{n\mathbf{k}}$ and eigenfunctions $\Psi_{\alpha n}(\mathbf{k})$ of the HF Hamiltonian, $\hat{H}_{HF} = \hat{H}_0 + \hat{V}_{HF}$. The $\mathbf{q} = \mathbf{0}$ self-energy for bond ℓ is

$$\tilde{P}^\ell = \sum_{\ell'} \tilde{V}^{\ell\ell'} \frac{1}{N} \sum_{\alpha\beta\mathbf{k}'} g_{\alpha\beta}^{\ell'}(\mathbf{k}')^* \Psi_{\beta n}^*(\mathbf{k}') \Psi_{\alpha n}(\mathbf{k}') f(E_{n\mathbf{k}'}). \quad (38)$$

Because the real part of Eq. (38) yields a homogeneous shift of the model parameters, we have retained only the imaginary part of $\tilde{P}^\ell$ in the self-consistency cycle. These calculations find that, for a range of V_{pd} values, the πLC phase is stable only for $p < p_{VH}$.

Figure 7 shows the amplitude of the current J_{pd} along the p-d bonds in the πLC phase. The current is measured in units of $et_{pd}/\hbar$, so $J_{pd} = 0.01$ corresponds to a current of $\sim 1\ \mu$A if $t_{pd} = 500$ meV. The current sets in at p_{VH} and its amplitude grows as hole doping is further reduced. The termination of the πLC phase at $p \approx p_{VH}$ is robust, as it is nearly independent of V_{pd}, and it is generally consistent with a recent experimental conclusion that the pseudogap phase is bounded by a Lifshitz transition [89]. However, the p dependence of J_{pd} is expected to be affected by strong correlations. In mean-field theory, the spectral gap associated with the πLC phase is proportional to the current amplitude. The HF self-energy Eq. (30) on the p-d bonds, which determines both the spectral gap and T_π, is proportional to V_{pd} and the generalized density ρ_{pd} between p and d orbitals, while the current in Eq. (31) is proportional to t_{pd} and ρ_{pd}. In the simplest picture, $t_{pd} \propto p$ so that the loop current amplitudes are renormalized downwards by strong correlations relative to the HF self-energy. This is similar to an effect predicted for strongly correlated superconductors: in conventional superconductors, the superconducting T_c is proportional to the superconducting gap Δ; however, super-fluid stiffness, and therefore T_c, is strongly reduced by strong correlations while the pairing gap remains large [90–94]. This suggests that the trends shown in Fig. 7(b) qualitatively capture the spectral gap but not the LC amplitude.

The πLC phase stops abruptly at low p at a value that does depend on V_{pd}; such a lower bound is not seen experimentally; however, the low-doping region of the phase diagram is complicated by strong correlations, the onset of a spin-glass phase, and by disorder [95,96], which are beyond the scope of our current calculations.

B. Charge instabilities in the loop-current state

To determine the leading instability within the πLC phase, we plot the T dependence of the leading eigenvalue $\chi(\mathbf{q})$ in Fig. 8 at $\mathbf{q}_0$ (loop current), $\mathbf{q}_1$ (diagonal dCDW), and $\mathbf{q}_2$ (axial dCDW). The susceptibility and its eigenvalues are now
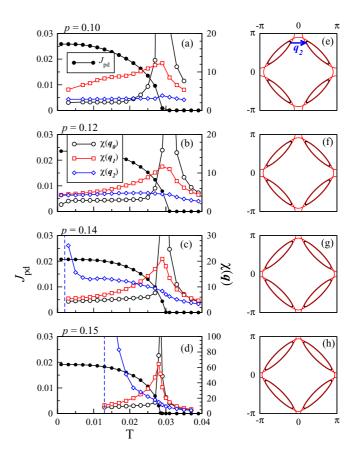

FIG. 8. Temperature evolution of the peaks in $\chi(\mathbf{q})$ at $\mathbf{q}_0$, $\mathbf{q}_1$, and $\mathbf{q}_2$ at four different fillings: (a) $p = 0.10$, (b) $p = 0.12$, (c) $p = 0.14$, (d) $p = 0.15$. The corresponding mean-field current along the p-d bond is also shown in each figure (left scale). The three wave vectors are $\mathbf{q}_0 = (0,0)$, $\mathbf{q}_1 = (q_1,q_1)$, $\mathbf{q}_2 = (q_2,0)$, where q_1 and q_2 are the peak positions along diagonal and axial directions. Fermi surfaces corresponding to the different hole fillings are shown in (e)–(h) for the normal state (red lines) and for the πLC state (black lines). As shown in (e), the axial wave vector connects tips of the hole pockets in the πLC phase.

calculated using the self-consistent HF Hamiltonian for the πLC phase. We focus on the region $p < p_{VH}$, where loop currents are found, and results are shown at five different dopings between $p = 0.10$ and $p = 0.17$. For reference, the Fermi surface and T dependence of J_{pd} are also shown for each doping.

At temperatures above T_π, $\chi(\mathbf{q})$ grows at all three $\mathbf{q}$ values as T is reduced. For $p \leqslant 0.15$, $\chi(\mathbf{q}_0)$ diverges first, signaling the onset of the πLC phase at T_π; $\chi(\mathbf{q}_0)$ then collapses rapidly in the ordered phase below T_π. For all hole densities in Fig. 8, the subleading peak is at $\mathbf{q}_1$ for $T > T_\pi$, indicating a tendency towards a diagonal dCDW. This peak at $\mathbf{q}_1$ is reduced by the onset of loop currents, however, which demonstrates a strong competition between diagonal dCDW and πLC order.

In contrast, there is only a weak competition between axial dCDW and πLC order. Above T_π, $\chi(\mathbf{q}_2)$ has positive curvature characteristic of growth towards a divergence; however, all curves show an inflection point slightly below T_π indicating that the onset of loop currents interrupts this divergence. Rather than being suppressed by loop currents, $\chi(\mathbf{q}_2)$ tends to saturate
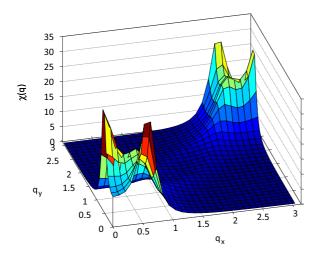
FIG. 9. Largest eigenvalue of the susceptibility matrix in the πLC phase. Results are at $p = 0.15$ for $V_{pd} = 3.0, V_{pp} = 1.0$, and at $T = 0.021$.

below T_π at a constant value [Figs. 8(a) and 8(b)], which can be an order of magnitude larger than at high T. At some doping levels [Figs. 8(c) and 8(d)], $\chi(\mathbf{q}_2)$ actually diverges below T_π, signaling the onset of an axially oriented dCDW. This is shown for $p = 0.15$ in Fig. 9, which shows the emergence of strong peaks at $\mathbf{q}_2 = (q_2, 0)$ and symmetry-related points. The corresponding eigenmode is illustrated in Fig. 10: there is a pronounced transfer of charge between Op orbitals, with an amplitude that is modulated along the y axis (right panel of Fig. 10). There is a smaller charge modulation on the Cu sites, amounting to $\sim$15% of the Op modulations. This is similar to the axial dCDW found previously for a phenomenological pseudogap model [26], and both the ordering wave vector and d-wave-like form factor of the charge modulations are consistent with experiments [21,22].
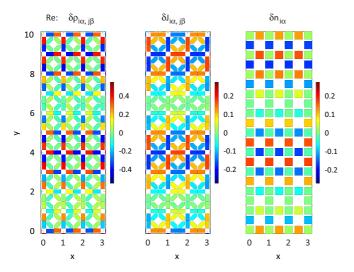
Concomitantly, the real part of $\delta\rho_{i\alpha, j\beta}$ (left panel in Fig. 10) inhomogeneously modulates the effective hopping strength, while the imaginary part corresponds to an incommensurate modulation of the bond current (middle panel in Fig. 10). We have checked that this incommensurate current pattern conserves charge at each vertex of the lattice. Indeed, it is straightforward to construct such a modulated current pattern by hand by requiring that current be conserved at each vertex. Current conservation at the Cu site at position $(m,n)a_0$, where a_0 is the primitive lattice constant, requires that the current coming in along the x axis must be carried out along the y axis, namely

$$\sum_{s=\pm 1} \left[I_x\left(m + \frac{s}{2}, n\right) + I_y\left(m, n + \frac{s}{2}\right) \right] = 0. \quad (39)$$

For a modulation wave vector $\mathbf{q}_2 = (0, q_2)$, this constraint implies

$$I_x\left(m + \tfrac{1}{2}, n\right) = I_0(-1)^{n+m} \cos(q_2 n a_0 + \theta), \quad (40)$$

where θ is an arbitrary constant phase, and

$$I_y\left(m, n + \frac{1}{2}\right) = -I_0(-1)^{n+m} \frac{\cos\left[q_2\left(n + \tfrac{1}{2}\right)a_0 + \theta\right]}{\cos(q_2 a_0/2)}. \quad (41)$$

Current conservation along the oxygen-oxygen bonds is simpler, as it requires only that the current be constant around each loop within a plaquette.

The weak competition between axial dCDW and πLC order has implications for the role of disorder. While the growth of critical diagonal dCDW fluctuations is interrupted at $T_\pi, \chi(\mathbf{q}_2)$ in some instances saturates below T_π at values that are substantially enhanced relative to the noninteracting case [where $\chi(\mathbf{q})$ is a number of order 1]. Figure 8(c), for example, is characterized by a wide temperature range below T_π where $\chi(\mathbf{q}_2)$ is more than an order of magnitude larger than in the noninteracting case. In this case crystalline disorder, for example due to dopant atoms, will induce short-range charge correlations with a strong $\mathbf{q}_2$ component even well above the charge-ordering transition at $T_{co} = 0.002$.

This is consistent with what is observed in the cuprates, where static short-range dCDW correlations develop at temperatures as high as $\sim$150 K [11,12], and true long-range dCDW order (with correlation lengths large enough to observe magneto-oscillation effects) only occurs at much lower temperatures, of order $\sim$50 K [9].

Finally, we note that the generalized susceptibility diverges simultaneously at symmetry-related points along the x and y directions (Fig. 9). Our linearized equations cannot determine whether uniaxial order, with ordering wave vector $(q_2, 0)$ or $(0, q_2)$, or biaxial (checkerboard) order in which both Fourier peaks are simultaneously present, is energetically preferred. Experimentally, domains of uniaxial order are seen in $Bi_2Sr_2CaCu_2O_{8+x}$ [21], while biaxial order is implied by magneto-oscillation experiments in $YBa_2Cu_3O_{6+x}$ [7].

In our calculations, the biaxial dCDW state is of particular interest because it breaks all mirror symmetries of the lattice, and coupled with the time-reversal-symmetry breaking of the πLC phase should generate a polar Kerr effect [97,98], similar to what has been measured in both $YBa_2Cu_3O_{6+x}$ [79] and $Pb_{0.55}Bi_{1.5}Sr_{1.6}La_{0.4}CuO_{6+\delta}$ [80]. This mechanism should

FIG. 10. Left panel: Induced shift in the real part of $\langle c_{i\alpha}^\dagger c_{j\beta}\rangle$, middle panel: the bond current, and right panel: the charge density. Parameters are as in Fig. 9. The charge modulations on the Cu sites are $\sim$15% of those on the O sites.

be distinguished from other proposals involving microscopic currents: in Refs. [97] and [98], the currents run along the edges of charge stripes, while in Ref. [99] a combination of staggered loop currents and d_{xy} bond order is proposed to explain the polar Kerr measurements. It remains unclear whether nanodomains of uniaxial order might also lead to a polar Kerr effect in our model.

IV. CONCLUSIONS

Motivated by the recent discovery of ubiquitous charge order within the pseudogap phase of underdoped cuprate superconductors, we have studied the development of d-charge density waves from within a pseudogap phase generated by a staggered π-loop current. Our main finding is that the πLC phase competes strongly with the dominant diagonal dCDW phase, and may weaken it sufficiently that axial dCDW order emerges as the leading charge instability. The resulting charge structure is consistent with x-ray scattering and STM experiments. A unique feature of the coexistence of dCDW and πLC order is the emergence of an incommensurate modulation of the loop current amplitude, illustrated in Fig. 10. If the dCDW has a checkerboard structure, then the resulting incommensurate current pattern breaks both mirror and time-reversal symmetries and should generate a polar Kerr effect.

APPENDIX A: HARTREE-FOCK APPROXIMATION AND BASIS FUNCTIONS

In this Appendix, we discuss technical details of our treatment of the interactions in the Hartree-Fock approximation. First, we give an explicit form for $V_{\alpha\beta}(\mathbf{q})$, defined by Eq. (10). Referring to Fig. 1, we obtain

$$
\begin{aligned}
V_{12}(\mathbf{q}) &= V_{45}(\mathbf{q}) = V_{24}(\mathbf{q}) = V_{51}(\mathbf{q}) = V_{pd}e^{iq_y/2}, \\
V_{21}(\mathbf{q}) &= V_{54}(\mathbf{q}) = V_{42}(\mathbf{q}) = V_{15}(\mathbf{q}) = V_{pd}e^{-iq_y/2}, \\
V_{13}(\mathbf{q}) &= V_{34}(\mathbf{q}) = V_{46}(\mathbf{q}) = V_{61}(\mathbf{q}) = V_{pd}e^{iq_x/2}, \\
V_{31}(\mathbf{q}) &= V_{43}(\mathbf{q}) = V_{64}(\mathbf{q}) = V_{16}(\mathbf{q}) = V_{pd}e^{-iq_x/2}, \\
V_{23}(\mathbf{q}) &= V_{32}(\mathbf{q}) = V_{56}(\mathbf{q}) = V_{65}(\mathbf{q}) \\
&= 2V_{pp}\cos\left(\frac{q_x - q_y}{2}\right), \\
V_{26}(\mathbf{q}) &= V_{62}(\mathbf{q}) = V_{53}(\mathbf{q}) = V_{35}(\mathbf{q}) \\
&= 2V_{pp}\cos\left(\frac{q_x + q_y}{2}\right),
\end{aligned}
\tag{A1}
$$

with all other matrix elements zero.

The correspondence between the basis function ℓ and the orbital label is given in Table I. From this table, we learn for

example that

$$
g^5_{\alpha\beta}(\mathbf{k}) = e^{ik_y/2}\delta_{\alpha,4}\delta_{\beta,5}.
\tag{A2}
$$

For this basis,

$$
\tilde{V}^{\ell\ell'}(\mathbf{q}) =
\begin{cases}
-V_{pd} & \ell = \ell'; \ell \in [1,16]; \\
-V_{pp} & \ell = \ell'; \ell \in [17,32]; \\
U_d & \ell = \ell' = 33,36; \\
U_p & \ell = \ell' = 34,35,37,38; \\
2V_{\alpha\beta}(\mathbf{q}) & \ell \neq \ell'; \ell,\ell' \in [33,38]; \\
0 & \text{otherwise.}
\end{cases}
\tag{A3}
$$

For the matrix elements containing $V_{\alpha\beta}(\mathbf{q}), \ell$ determines α and ℓ' determines β, with the connection given by Table I.

APPENDIX B: SYMMETRIES OF THE SUSCEPTIBILITY

1. Hermiticity of $\tilde{\mathbf{X}}(\mathbf{q})$

From Eq. (26), we obtain the relationship for the static susceptibility

$$
\tilde{X}^{\ell\ell'}_0(\mathbf{q})^* = \tilde{X}^{\ell'\ell}_0(\mathbf{q}),
\tag{B1}
$$

or, in matrix notation, $\tilde{\mathbf{X}}_0(\mathbf{q})^\dagger = \tilde{\mathbf{X}}_0(\mathbf{q})$. Since $\tilde{\mathbf{V}}(\mathbf{q})^\dagger = \tilde{\mathbf{V}}(\mathbf{q})$, it also follows that

$$
\tilde{\mathbf{X}}(\mathbf{q})^\dagger = \tilde{\mathbf{X}}(\mathbf{q}).
\tag{B2}
$$

2. Relation between $\tilde{\mathbf{X}}(\mathbf{q})$ and $\tilde{\mathbf{X}}(-\mathbf{q})$

It also follows from Eq. (26) that

$$
\tilde{X}^{\ell\ell'}_0(-\mathbf{q}) = \tilde{X}^{\overline{\ell}'\overline{\ell}}_0(\mathbf{q}) = \left[\tilde{X}^{\overline{\ell\ell}'}_0(\mathbf{q})\right]^*,
\tag{B3}
$$

where $\overline{\ell}$ represents the same bond as ℓ, but oriented in the opposite sense. Let $\mathbf{T}$ be the unitary matrix that swaps bonds to the opposite orientation; we obtain the matrix representation $\tilde{\mathbf{X}}_0(-\mathbf{q}) = \mathbf{T}\tilde{\mathbf{X}}_0(\mathbf{q})\mathbf{T}^\dagger$. Because

$$
\tilde{\mathbf{V}}(\mathbf{q}) = \mathbf{T}\tilde{\mathbf{V}}(\mathbf{q})\mathbf{T}^\dagger, \quad \tilde{\mathbf{V}}(-\mathbf{q}) = \tilde{\mathbf{V}}(\mathbf{q})^*,
\tag{B4}
$$

it also happens that

$$
\tilde{\mathbf{X}}(-\mathbf{q}) = \mathbf{T}\tilde{\mathbf{X}}(\mathbf{q})^*\mathbf{T}^\dagger.
\tag{B5}
$$

For the labeling of the bonds shown in Table I,

$$
\mathbf{T} =
\begin{bmatrix}
\mathbf{0}_{8\times8} & \mathbf{1}_{8\times8} & \mathbf{0}_{8\times8} & \mathbf{0}_{8\times8} & \mathbf{0}_{8\times6} \\
\mathbf{1}_{8\times8} & \mathbf{0}_{8\times8} & \mathbf{0}_{8\times8} & \mathbf{0}_{8\times8} & \mathbf{0}_{8\times6} \\
\mathbf{0}_{8\times8} & \mathbf{0}_{8\times8} & \mathbf{0}_{8\times8} & \mathbf{1}_{8\times8} & \mathbf{0}_{8\times6} \\
\mathbf{0}_{8\times8} & \mathbf{0}_{8\times8} & \mathbf{1}_{8\times8} & \mathbf{0}_{8\times8} & \mathbf{0}_{8\times6} \\
\mathbf{0}_{6\times8} & \mathbf{0}_{6\times8} & \mathbf{0}_{6\times8} & \mathbf{0}_{6\times8} & \mathbf{1}_{6\times6}
\end{bmatrix}.
\tag{B6}
$$

Note that $\mathbf{T}^\dagger = \mathbf{T}$ in this case.

3. Eigenvectors of $\tilde{\mathbf{X}}(\mathbf{q})$

Equation (B5) implies that the eigenvalue equation, $\tilde{\mathbf{X}}(\mathbf{q})\mathbf{v_q} = \chi(\mathbf{q})\mathbf{v_q}$, transforms as

$$
\mathbf{T}\tilde{\mathbf{X}}(\mathbf{q})^*\mathbf{T}^\dagger\mathbf{T}\mathbf{v_q^*} = \chi(\mathbf{q})\mathbf{T}\mathbf{v_q^*},
\tag{B7}
$$

$$
\tilde{\mathbf{X}}(-\mathbf{q})\mathbf{T}\mathbf{v_q^*} = \chi(\mathbf{q})\mathbf{T}\mathbf{v_q^*}.
\tag{B8}
$$

Because $\chi(-\mathbf{q}) = \chi(\mathbf{q})$, it follows that $\mathbf{T}\mathbf{v}_\mathbf{q}^* = e^{i\theta}\mathbf{v}_{-\mathbf{q}}$, where θ is an arbitrary phase. Without loss of generality, we take $\theta = 0$ and

$$\mathbf{T}\mathbf{v}_\mathbf{q}^* = \mathbf{v}_{-\mathbf{q}}. \tag{B9}$$

4. Simplification of the equation for $\delta\rho_{i\alpha, j\beta}$

Equation (35) gives the induced generalized charge density

$$\delta\tilde{\boldsymbol{\rho}}(\mathbf{q}) = -\tilde{\mathbf{X}}(-\mathbf{q})^*\tilde{\boldsymbol{\phi}}(-\mathbf{q})^*. \tag{B10}$$

Using the symmetry relations above along with the Hermiticity condition (21), Eq. (B10) becomes

$$\tilde{\boldsymbol{\rho}}(\mathbf{q}) = -\mathbf{T}\tilde{\mathbf{X}}(\mathbf{q})\tilde{\boldsymbol{\phi}}(\mathbf{q}). \tag{B11}$$

Letting ℓ correspond to the bond $(i\alpha, j\beta)$,

$$\delta\rho_{i\alpha, j\beta} = \delta\tilde{\rho}^\ell(\mathbf{q})e^{i\frac{\mathbf{q}}{2}\cdot(\mathbf{r}_{i\alpha}+\mathbf{r}_{j\beta})} + \delta\tilde{\rho}^\ell(-\mathbf{q})e^{-i\frac{\mathbf{q}}{2}\cdot(\mathbf{r}_{i\alpha}+\mathbf{r}_{j\beta})}$$

$$= -e^{i\frac{\mathbf{q}}{2}\cdot(\mathbf{r}_{i\alpha}+\mathbf{r}_{j\beta})}[\mathbf{T}\tilde{\mathbf{X}}(\mathbf{q})\tilde{\boldsymbol{\phi}}(\mathbf{q})]^\ell$$

$$- e^{-i\frac{\mathbf{q}}{2}\cdot(\mathbf{r}_{i\alpha}+\mathbf{r}_{j\beta})}[\tilde{\mathbf{X}}(\mathbf{q})^*\tilde{\boldsymbol{\phi}}(\mathbf{q})^*]^\ell. \tag{B12}$$

If $\tilde{\boldsymbol{\phi}}(\mathbf{q})$ is proportional to an eigenvector of $\tilde{\mathbf{X}}(\mathbf{q})$ with real eigenvalue $\chi(\mathbf{q})$, then

$$\delta\rho_{i\alpha, j\beta} = -\chi(\mathbf{q})\{e^{i\frac{\mathbf{q}}{2}\cdot(\mathbf{r}_{i\alpha}+\mathbf{r}_{j\beta})}[\mathbf{T}\tilde{\boldsymbol{\phi}}(\mathbf{q})]^\ell + e^{-i\frac{\mathbf{q}}{2}\cdot(\mathbf{r}_{i\alpha}+\mathbf{r}_{j\beta})}[\tilde{\boldsymbol{\phi}}(\mathbf{q})^*]^\ell\}$$

$$= -\chi(\mathbf{q})\{e^{i\frac{\mathbf{q}}{2}\cdot(\mathbf{r}_{i\alpha}+\mathbf{r}_{j\beta})}\tilde{\phi}^{\overline{\ell}}(\mathbf{q}) + e^{-i\frac{\mathbf{q}}{2}\cdot(\mathbf{r}_{i\alpha}+\mathbf{r}_{j\beta})}\tilde{\phi}^\ell(\mathbf{q})^*\}. \tag{B13}$$

Taking $\tilde{\phi}^{\overline{\ell}}(\mathbf{q}) = \varphi_\mathbf{q}v_\mathbf{q}^{\overline{\ell}}$, we obtain Eq. (36).

---

[1] J. E. Hoffman, E. W. Hudson, K. M. Lang, V. Madhavan, H. Eisaki, S. Uchida, and J. C. Davis, Science **295**, 466 (2002).

[2] Y. Kohsaka, C. Taylor, K. Fujita, A. Schmidt, C. Lupien, T. Hanaguri, M. Azuma, M. Takano, H. Eisaki, H. Takagi *et al.*, Science **315**, 1380 (2007).

[3] W. D. Wise, M. C. Boyer, K. Chatterjee, T. Kondo, T. Takeuchi, H. Ikuta, Y. Wang, and E. W. Hudson, Nat. Phys. **4**, 696 (2008).

[4] R. Daou, J. Chang, D. LeBoeuf, O. Cyr-Choinière, F. Laliberté, N. Doiron-Leyraud, B. J. Ramshaw, R. Liang, D. A. Bonn, W. N. Hardy *et al.*, Nature (London) **463**, 519 (2010).

[5] J. Chang, R. Daou, C. Proust, D. LeBoeuf, N. Doiron-Leyraud, F. Laliberté, B. Pingault, B. J. Ramshaw, R. Liang, D. A. Bonn *et al.*, Phys. Rev. Lett. **104**, 057005 (2010).

[6] J. Chang, N. Doiron-Leyraud, F. Laliberté, R. Daou, D. LeBoeuf, B. Ramshaw, R. Liang, D. Bonn, W. Hardy, C. Proust *et al.*, Phys. Rev. B **84**, 014507 (2011).

[7] S. E. Sebastian, N. Harrison, and G. Lonzarich, Rep. Prog. Phys. **75**, 102501 (2012).

[8] N. Harrison and S. E. Sebastian, New J. Phys. **14**, 095023 (2012).

[9] T. Wu, H. Mayaffre, S. Krämer, M. Horvatić, C. Berthier, W. N. Hardy, R. Liang, D. A. Bonn, and M.-H. Julien, Nature (London) **477**, 191 (2011).

[10] T. Wu, H. Mayaffre, S. Krämer, M. Horvatić, C. Berthier, P. L. Kuhns, A. P. Reyes, R. Liang, W. N. Hardy, D. A. Bonn *et al.*, Nat. Commun. **4**, 2113 (2013).

[11] G. Ghiringhelli, M. Le Tacon, M. Minola, S. Blanco-Canosa, C. Mazzoli, N. B. Brookes, G. M. De Luca, A. Frano, D. G. Hawthorn, F. He *et al.*, Science **337**, 821 (2012).

[12] J. Chang, E. Blackburn, A. T. Holmes, N. B. Christensen, J. Larsen, J. Mesot, R. Liang, D. A. Bonn, W. N. Hardy, A. Watenphul *et al.*, Nat. Phys. **8**, 871 (2012).

[13] E. Blackburn, J. Chang, M. Hücker, A. T. Holmes, N. B. Christensen, R. Liang, D. A. Bonn, W. N. Hardy, U. Rütt, O. Gutowski *et al.*, Phys. Rev. Lett. **110**, 137004 (2013).

[14] S. Blanco-Canosa, A. Frano, T. Loew, Y. Lu, J. Porras, G. Ghiringhelli, M. Minola, C. Mazzoli, L. Braicovich, E. Schierle *et al.*, Phys. Rev. Lett. **110**, 187001 (2013).

[15] M. Hücker, N. B. Christensen, A. T. Holmes, E. Blackburn, E. M. Forgan, R. Liang, D. A. Bonn, W. N. Hardy, O. Gutowski, M. v. Zimmermann *et al.*, Phys. Rev. B **90**, 054514 (2014).

[16] N. Doiron-Leyraud, S. Lepault, O. Cyr-Choinière, B. Vignolle, G. Grissonnanche, F. Laliberté, J. Chang, N. Barišić, M. K. Chan, L. Ji *et al.*, Phys. Rev. X **3**, 021019 (2013).

[17] N. Barišić, S. Badoux, M. K. Chan, C. Dorow, W. Tabis, B. Vignolle, G. Yu, J. Béard, X. Zhao, C. Proust *et al.*, Nat. Phys. **9**, 761 (2013).

[18] W. Tabis, Y. Li, M. Le Tacon, L. Braicovich, A. Kreyssig, M. Minola, G. Dellea, E. Weschke, M. J. Veit, M. Ramazanoglu *et al.*, Nat. Commun. **5**, 5875 (2014).

[19] E. H. da Silva Neto, R. Comin, F. He, R. Sutarto, Y. Jiang, R. L. Greene, G. A. Sawatzky, and A. Damascelli, Science **347**, 282 (2015).

[20] A. Mesaros, K. Fujita, H. Eisaki, S. Uchida, J. C. Davis, S. Sachdev, J. Zaanen, M. J. Lawler, and E.-A. Kim, Science **333**, 426 (2011).

[21] K. Fujita, M. H. Hamidian, S. D. Edkins, C. K. Kim, Y. Kohsaka, M. Azuma, M. Takano, H. Takagi, H. Eisaki, S.-i. Uchida *et al.*, Proc. Natl. Acad. Sci. USA **111**, E3026 (2014).

[22] R. Comin, R. Sutarto, F. He, E. d. S. Neto, L. Chauviere, A. Frano, R. Liang, W. N. Hardy, D. Bonn, Y. Yoshida *et al.*, Nat. Mater. **14**, 796 (2015).

[23] A. J. Achkar, F. He, R. Sutarto, C. McMahon, M. Zwiebler, M. Hücker, G. D. Gu, R. Liang, D. A. Bonn, W. N. Hardy *et al.*, Nat. Mater., doi:10.1038/nmat4568 (2016).

[24] M. H. Fischer and E.-A. Kim, Phys. Rev. B **84**, 144502 (2011).

[25] S. Bulut, W. A. Atkinson, and A. P. Kampf, Phys. Rev. B **88**, 155132 (2013).

[26] W. A. Atkinson, A. P. Kampf, and S. Bulut, New J. Phys. **17**, 013025 (2015).

[27] M. H. Fischer, S. Wu, M. Lawler, A. Paramekanti, and E.-A. Kim, New J. Phys. **16**, 093057 (2014).

[28] M. Vojta, Adv. Phys. **58**, 699 (2009).

[29] V. Thampy, S. Blanco-Canosa, M. García-Fernández, M. P. M. Dean, G. D. Gu, M. Först, T. Loew, B. Keimer, M. Le Tacon, S. B. Wilkins, and J. P. Hill, Phys. Rev. B **88**, 024505 (2013).

[30] R. Comin, A. Frano, M. M. Yee, Y. Yoshida, H. Eisaki, E. Schierle, E. Weschke, R. Sutarto, F. He, A. Soumyanarayanan *et al.*, Science **343**, 390 (2014).

[31] M. H. Hamidian, S. D. Edkins, C. K. Kim, J. C. Davis, A. P. Mackenzie, H. Eisaki, S. Uchida, M. J. Lawler, E. A. Kim, S. Sachdev *et al.*, Nat. Phys. **12**, 150 (2016).

[32] H. Alloul, P. Mendels, H. Casalta, J. F. Marucco, and J. Arabski, Phys. Rev. Lett. **67**, 3140 (1991).

[33] G.-Q. Zheng *et al.*, J. Phys. Soc. Jpn. **62**, 2591 (1993).

[34] G.-Q. Zheng, T. Odaguchi, Y. Kitaoka, K. Asayama, Y. Kodama, K. Mizuhashi, and S. Uchida, Physica C **263**, 367 (1996).

[35] H. Alloul, J. Bobroff, M. Gabay, and P. J. Hirschfeld, Rev. Mod. Phys. **81**, 45 (2009).

[36] W. A. Atkinson and A. P. Kampf, Phys. Rev. B **91**, 104509 (2015).

[37] D. Chowdhury and S. Sachdev, Phys. Rev. B **90**, 245136 (2014).

[38] G. Nikšić, D. K. Sunko, and S. Barišić, Phys. B (Amsterdam, Neth.) **460**, 218 (2015).

[39] A. Thomson and S. Sachdev, Phys. Rev. B **91**, 115142 (2015).

[40] M. A. Metlitski and S. Sachdev, Phys. Rev. B **82**, 075128 (2010).

[41] M. Metlitski and S. Sachdev, New J. Phys. **12**, 105007 (2010).

[42] K. B. Efetov, H. Meier, and C. Pépin, Nat. Phys. **9**, 442 (2013).

[43] H. Meier, M. Einenkel, C. Pépin, and K. B. Efetov, Phys. Rev. B **88**, 020506 (2013).

[44] Y. Wang and A. Chubukov, Phys. Rev. B **90**, 035149 (2014).

[45] T. Holder and W. Metzner, Phys. Rev. B **85**, 165130 (2012).

[46] C. Husemann and W. Metzner, Phys. Rev. B **86**, 085113 (2012).

[47] M. Bejas, A. Greco, and H. Yamase, Phys. Rev. B **86**, 224509 (2012).

[48] J. D. Sau and S. Sachdev, Phys. Rev. B **89**, 075129 (2014).

[49] D. Chowdhury and S. Sachdev, Phys. Rev. B **90**, 134516 (2014).

[50] S. Feng, D. Gao, and H. Zhao, Philos. Mag. B **96**, 1245 (2016).

[51] S. Sachdev and R. La Placa, Phys. Rev. Lett. **111**, 027202 (2013).

[52] Y. Yamakawa and H. Kontani, Phys. Rev. Lett. **114**, 257001 (2015).

[53] J. Bauer and S. Sachdev, Phys. Rev. B **92**, 085134 (2015).

[54] Y. Wang, D. F. Agterberg, and A. Chubukov, Phys. Rev. Lett. **114**, 197001 (2015).

[55] Y. Wang, D. F. Agterberg, and A. Chubukov, Phys. Rev. B **91**, 115103 (2015).

[56] L. E. Hayward, D. G. Hawthorn, R. G. Melko, and S. Sachdev, Science **343**, 1336 (2014).

[57] C. Pépin, V. S. de Carvalho, T. Kloss, and X. Montiel, Phys. Rev. B **90**, 195207 (2014).

[58] T. Kloss, X. Montiel, and C. Pépin, Phys. Rev. B **91**, 205124 (2015).

[59] B. Kyung, S. S. Kancharla, D. Senechal, A. M. S. Tremblay, M. Civelli, and G. Kotliar, Phys. Rev. B **73**, 165114 (2006).

[60] O. Gunnarsson, T. Schäfer, J. P. F. LeBlanc, E. Gull, J. Merino, G. Sangiovanni, G. Rohringer, and A. Toschi, Phys. Rev. Lett. **114**, 236402 (2015).

[61] A. Shekhter, B. J. Ramshaw, R. Liang, W. N. Hardy, D. A. Bonn, F. F. Balakirev, R. D. McDonald, J. B. Betts, S. C. Riggs, and A. Migliori, Nature (London) **498**, 75 (2013).

[62] B. J. Ramshaw, S. E. Sebastian, R. D. McDonald, J. Day, B. S. Tan, Z. Zhu, J. B. Betts, R. Liang, D. A. Bonn, W. N. Hardy *et al.*, Science **348**, 317 (2015).

[63] J. R. Cooper, J. W. Loram, I. Kokanović, J. G. Storey, and J. L. Tallon, Phys. Rev. B **89**, 201104 (2014).

[64] C. Castellani, C. Di Castro, and M. Grilli, Z. Phys. B **103**, 137 (1997).

[65] C. M. Varma, Phys. Rev. B **55**, 14554 (1997).

[66] J. L. Tallon and J. W. Loram, Physica C **349**, 53 (2001).

[67] L. Taillefer, Annu. Rev. Condens. Matter Phys. **1**, 51 (2010).

[68] I. Affleck and J. B. Marston, Phys. Rev. B **37**, 3774 (1988).

[69] Z. Wang, G. Kotliar, and X.-F. Wang, Phys. Rev. B **42**, 8690 (1990).

[70] S. Chakravarty, R. B. Laughlin, D. K. Morr, and C. Nayak, Phys. Rev. B **63**, 094503 (2001).

[71] P. A. Lee, N. Nagaosa, and X.-G. Wen, Rev. Mod. Phys. **78**, 17 (2006).

[72] R. B. Laughlin, Phys. Rev. Lett. **112**, 017004 (2014).

[73] S. Bulut, A. P. Kampf, and W. A. Atkinson, Phys. Rev. B **92**, 195140 (2015).

[74] H. A. Mook, P. Dai, S. M. Hayden, A. Hiess, J. W. Lynn, S.-H. Lee, and F. Doğan, Phys. Rev. B **66**, 144513 (2002).

[75] H. A. Mook, P. Dai, and F. Doğan, Phys. Rev. Lett. **88**, 097004 (2002).

[76] C. Stock, W. J. L. Buyers, Z. Tun, R. Liang, D. Peets, D. Bonn, W. N. Hardy, and L. Taillefer, Phys. Rev. B **66**, 024505 (2002).

[77] H. A. Mook, P. Dai, S. M. Hayden, A. Hiess, S.-H. Lee, and F. Dogan, Phys. Rev. B **69**, 134509 (2004).

[78] J. E. Sonier, V. Pacradouni, S. A. Sabok-Sayr, W. N. Hardy, D. A. Bonn, R. Liang, and H. A. Mook, Phys. Rev. Lett. **103**, 167002 (2009).

[79] J. Xia, E. Schemm, G. Deutscher, S. A. Kivelson, D. A. Bonn, W. N. Hardy, R. Liang, W. Siemons, G. Koster, M. M. Fejer *et al.*, Phys. Rev. Lett. **100**, 127002 (2008).

[80] R.-H. He, M. Hashimoto, H. Karapetyan, J. D. Koralek, J. P. Hinton, J. P. Testaud, V. Nathan, Y. Yoshida, H. Yao, K. Tanaka *et al.*, Science **331**, 1579 (2011).

[81] M. S. Hybertsen, M. Schlüter, and N. E. Christensen, Phys. Rev. B **39**, 9028 (1989).

[82] C. Weber, K. Haule, and G. Kotliar, Phys. Rev. B **78**, 134519 (2008).

[83] I. M. Vishik, W. S. Lee, F. Schmitt, B. Moritz, T. Sasagawa, S. Uchida, K. Fujita, S. Ishida, C. Zhang, T. P. Devereaux *et al.*, Phys. Rev. Lett. **104**, 207002 (2010).

[84] F. C. Zhang and T. M. Rice, Phys. Rev. B **37**, 3759(R) (1988).

[85] A. Damascelli, Z. Hussain, and Z.-X. Shen, Rev. Mod. Phys. **75**, 473 (2003).

[86] T. A. Maier, M. Jarrell, T. C. Schulthess, P. R. C. Kent, and J. B. White, Phys. Rev. Lett. **95**, 237001 (2005).

[87] B. Kyung and A.-M. S. Tremblay, Phys. Rev. Lett. **97**, 046402 (2006).

[88] M. Capone and G. Kotliar, Phys. Rev. B **74**, 054513 (2006).

[89] S. Benhabib, A. Sacuto, M. Civelli, I. Paul, M. Cazayous, Y. Gallais, M. A. Méasson, R. D. Zhong, J. Schneeloch, G. D. Gu *et al.*, Phys. Rev. Lett. **114**, 147001 (2015).

[90] P. W. Anderson, Science **235**, 1196 (1987).

[91] F. C. Zhang, C. Gros, T. M. Rice, and H. Shiba, Supercond. Sci. Technol. **1**, 36 (1988).

[92] C. Gros, Phys. Rev. B **38**, 931 (1988).

[93] A. Paramekanti, M. Randeria, and N. Trivedi, Phys. Rev. B **70**, 054504 (2004).

[94] K. Haule and G. Kotliar, Phys. Rev. B **76**, 104509 (2007).

[95] G. Alvarez and E. Dagotto, Phys. Rev. Lett. **101**, 177001 (2008).

[96] W. A. Atkinson, Phys. Rev. B **75**, 024510 (2007).

[97] Y. Wang, A. Chubukov, and R. Nandkishore, Phys. Rev. B **90**, 205130 (2014).

[98] M. Gradhand, I. Eremin, and J. Knolle, Phys. Rev. B **91**, 060512(R) (2015).

[99] G. Sharma, S. Tewari, P. Goswami, V. M. Yakovenko, and S. Chakravarty, Phys. Rev. B **93**, 075156 (2016).